CHAPTER 5

Electrical and Optical Properties of PQT-12 Based Organic Thin Film Transistor Fabricated by Floating Film Transfer Method*

Contents

*Part of this work has been published as:

1. Chandan Kumar et al., "Electrical and optical characteristics of PQT-12-based organic TFTs fabricated by floating-film transfer method," *IEEE Transactions on Nanotechnology*, vol. 17, no. 6, pp. 1111–1117, 2018.

CHAPTER 5

Electrical and Optical Properties of PQT-12 Based Organic Thin Film Transistor Fabricated by Floating Film Transfer Method

5.1 Introduction

The electrical and gas sensing properties of the PQT-12 thin film based OTFT using the floating-film transfer method (FTM) have been investigated in Chapter-4. It is also discussed in Chapter-1 that conducting polymers based OTFT may also be explored for the photodetection applications [4], [82], [84], [85], [140]. Under illumination, photoexcitons are generated in the polymer film which shifts the Fermi level close to the HOMO (or LUMO) level in the p-type (n-type) polymers [83]. This enhances the field effect mobility and hence the on-current of the OTFTs. It is also shown that the FTM coated polymer films have better electrical and optical responses over the conventional spin-coated polymer films [147]. Wasapinyokul et al. [149] reported a spin-coated PQT-12 polymer based phototransistor with a very low field-effect mobility of 1.1×10^{-3} $cm^2/V\text{-}s$ and the maximum responsivity of 6.6 A/W at 525 nm under 3 $\mu W/cm^2$ incident illumination intensity. Since both the FTM and PQT-12 are relatively new in their own categories, the present chapter investigates the optoelectronic properties of the PQT-12 based OTFT considered in Chapter-4. The outline of the rest of this chapter is as follows:

Section 5.2 includes the brief of experimental details of the fabrication of PQT-12 based OTFT using the FTM technique. The electrical and optical properties of the OTFT sensor are presented in section 5.3. Finally, section 5.4 includes the summary and conclusion of this chapter.

5.2 Experimental Details

5.2.1 Thin Film Deposition and OTFT Fabrication

The bottom-gate and top-contact structure of the OTFT has been fabricated on heavily doped p-type silicon <100> substrate coated with a thermally grown 300 nm SiO_2 layer on it. The surface of the as-grown SiO_2 (on the silicon substrate) has been modified by immersing the sample in the 1 mM solution of OTS in toluene for 12 hours. Subsequently, the substrates are washed in toluene ultrasonically and dried at 140°C for 1 hour followed by slow cooling to room temperature. To obtain a ~20 nm PQT-12 film, the solution of 5 mg PQT-12 is first dissolved in 1 ml anhydrous chloroform. Then 15 µl of this hydrophobic solution of PQT-12 is dropped on the hydrophilic solution of ethylene glycol (EG) and glycerol (G) in 1:1 ratio in a petri-dish. A uniform and self-assembled PQT-12 film is then formed over the hydrophilic solution [112]. The PQT-12 film is then stamped on OTS modified Si/SiO_2 substrate. The stamped PQT-12 film is washed by methanol and then dried at 80°C under nitrogen environment for 1 hour and cooled down slowly to room temperature. Then, 60 nm thin gold films are deposited on the PQT-12 film for forming the source and drain with a 30 µm channel length (*L*) and 1 mm width (*W*) as shown in OTFT cross-sectional image in Figure 5.1.

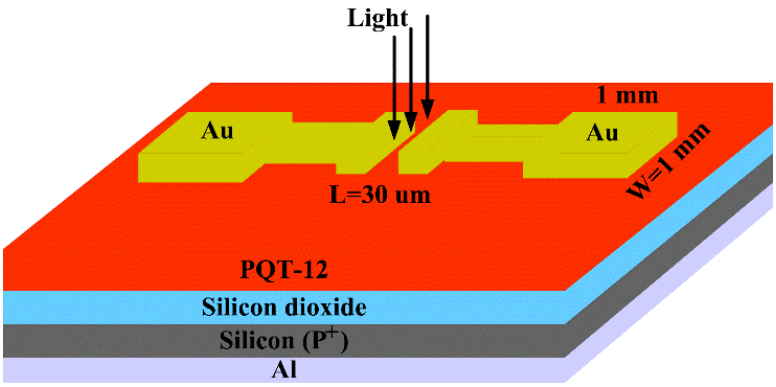

Figure 5.1: The cross-sectional device structure of as-fabricated PQT-12 based OTFT.

5.3 Results and Discussion

In this section, the results of thin film and electrical as well as optical characterization of PQT-12 based devices are presented.

5.3.1 Thin Film Characterization

The electrical and optical properties of the polymer-based films mainly depend on the macromolecule structures [27] and orientations [28] of the polymer in the film. The point-symmetrical substituents structure formed in the PQT-12 due to free sliding of macromolecules in the film [27], [28], which leads to the formation of the well-oriented film when no external force is applied on the free sliding motion of macromolecules. The macromolecule structures can move freely in the liquid crystalline phase of PQT-12 obtained by FTM technique on liquid substrates (EG:G). As a result, PQT-12 films grown by the FTM exhibit better electrical and optical properties with enhanced stability [147] than those of the spin-coated PQT-12 films [28], [105]. Figure 5.2 compares the optical absorbance characteristics of the FTM and spin-coating based PQT-12 films deposited on glass substrates. The FTM based film clearly shows higher shoulder peak at ~583 nm than that of the spin-coated PQT-12 film due to well aligned and self-assembled film characteristics [28]. The FTM film shows optical anisotropy [28] with dichroic ratio (DR) of 1.73 estimated from absorption spectra under polarized light shown in inset of Figure 5.2. The photoluminescence (PL) of the FTM and spin-coated films shown in Figure 5.3 reveals higher and sharper luminescence peaks of FTM film than the spin-coated PQT-12 film at 612 and 661 nm. Further, the trailing edge of the FTM film is decreased at a higher rate than the spin-coated film. The spin-coated PQT-12 films have higher luminescence at ~700 nm (at low energy) possibly due to trapping sites [178]. The faster rate of decrease of trailing edges in FTM films

confirms the lower charge trapping sites in FTM films as compared to the spin-coated PQT-12 films. The lower charge trapping sites in the FTM films improve the performance by increasing the response time of the device. The surface morphology of PQT-12 film deposited on the OTS modified Si/SiO_2 substrates using spin-coating and FTM are compared in terms of the AFM images as shown in Figure 5.4 (a) and (b), respectively. Clearly, the FTM films show higher surface roughness over spin-coated films. Since the increased surface roughness increases the surface-to-volume ratio, the effective area for optical absorbance in the FTM based films may be assumed to be larger than that of the spin-coated PQT-12 films under study. The roughness parameters obtained for both the spin-coated and FTM film have been listed in Table 5.1.

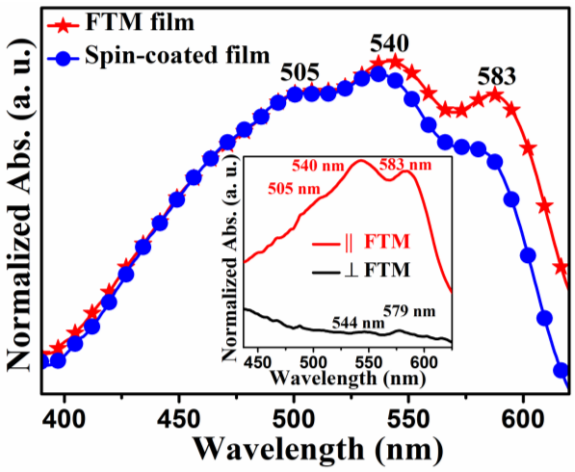

Figure 5.2: Optical absorbance in spin-coated and FTM coated PQT-12 films. Inset image shows the absorption in parallel and perpendicular aligned FTM film using polarized light.

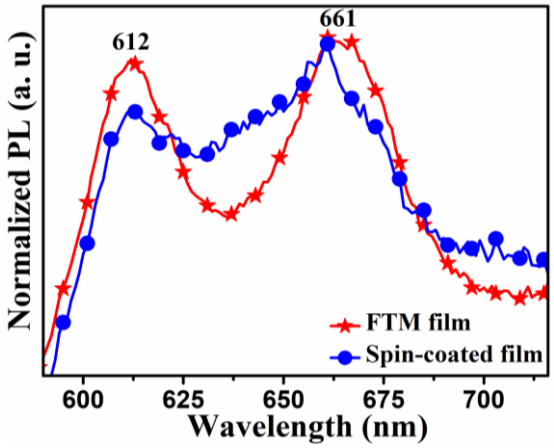

Figure 5.3: Photoluminance in the spin-coated and FTM coated PQT-12 films.

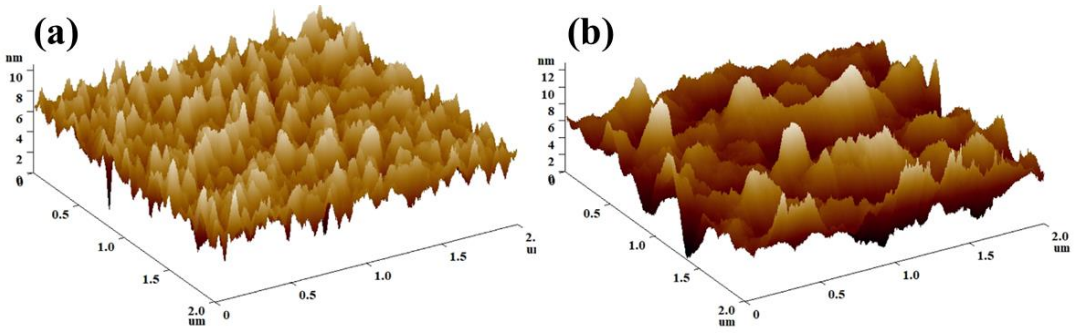

Figure 5.4: AFM 3D topography images of (a) spin-coated PQT-12 film and (b) FTM Coated PQT-12 film.

Table 5.1: Surface parameters of spin-coated and FTM coated PQT-12 films.

Surface parameters	Spin-coated film	FTM film
Average roughness (nm)	0.8	1.3
RMS roughness (nm)	1.0	1.7
Peak to peak spacing (nm)	10.6	12.9

5.3.2 Electrical Characterization

First, we have studied the output and transfer characteristics of the fabricated FTM coated PQT-12 based OTFT under dark condition. The output characteristics (drain current (I_D) versus drain-to-source (V_{DS})) are shown in Figure 5.5 for different values of gate-to-source voltage (V_{GS}). The drain current is saturated for much higher drain voltages than the conventional semiconductor-based transistors. The OTFT performance

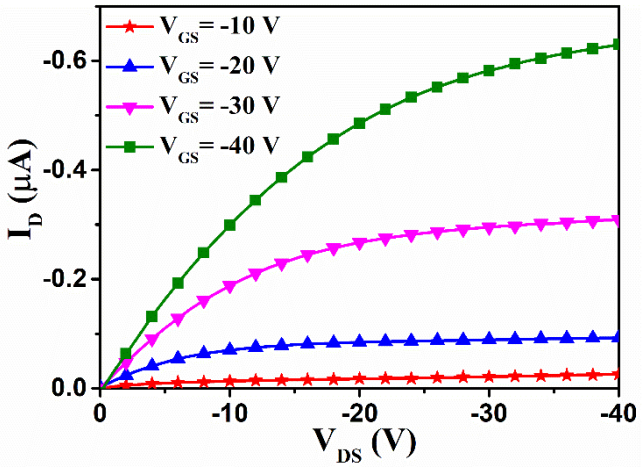

Figure 5.5: Output characteristics of the PQT-12 thin film based OTFT under dark condition.

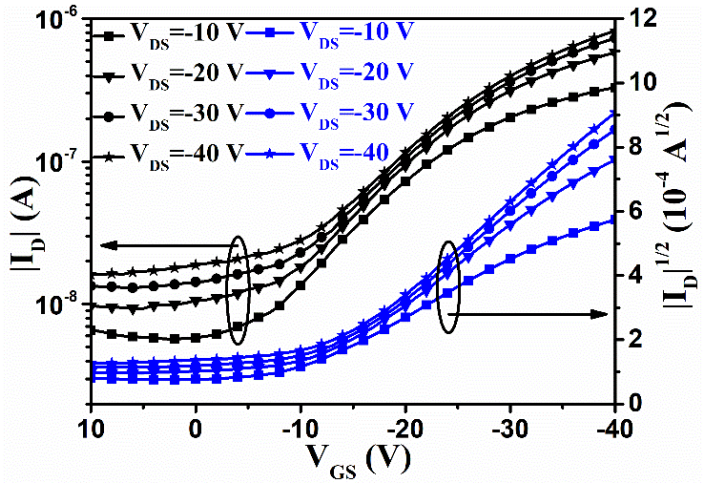

Figure 5.6: Transfer characteristics of the PQT-12 thin film based OTFT under dark condition.

parameters have been calculated from the transfer characteristics (I_D vs. V_{GS}) shown in Figure 5.6 by using the following drain current equation in saturation region:

$$I_{D,d} = \frac{W}{2L}\mu C_i \left(V_{GS} - V_{th}\right)^2 \tag{5.1}$$

We thus write,

$$\sqrt{I_{D,d}} = \sqrt{\frac{W}{2L}\mu C_i}\left(V_{GS} - V_{th}\right) = P\left(V_{GS} - Q\right) \tag{5.2}$$

where, $I_{D,d}$ is the drain current, μ is the field effect mobility, V_{th} is the threshold voltage, C_i is the insulator capacitance, P is the slope of $\sqrt{I_{D,d}}$ vs. V_{GS} characteristic and Q is the intercept of $\sqrt{I_{D,d}}$ vs. V_{GS} curve on the V_{GS} axis under dark condition. The field effect mobility and threshold voltage are calculated as 7.8×10^{-2} cm^2/Vs and -8.1 V, respectively, under the dark condition of the device.

5.3.3 Optical Characterization

The output characteristics under illumination of the OTFT using FTM based PQT-12 film have been shown in Figure 5.7 for a fixed V_{GS} of -40 V but different wavelengths of light. The maximum drain current is observed for 540 nm of light where the PQT-12

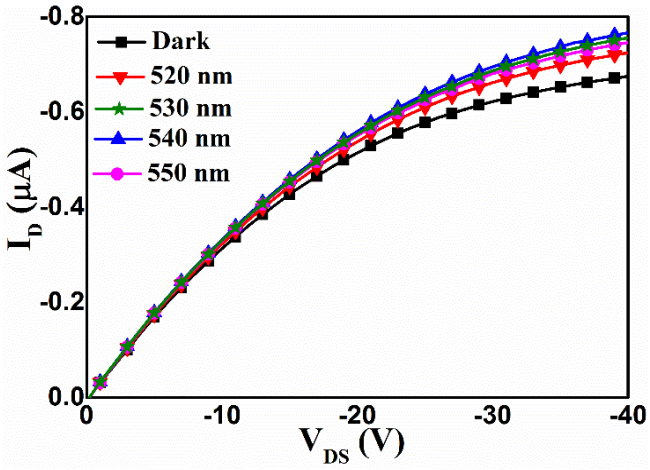

Figure 5.7: Output characteristics of the OTFT under illumination of 200 μW/cm^2 light intensity at different wavelength.

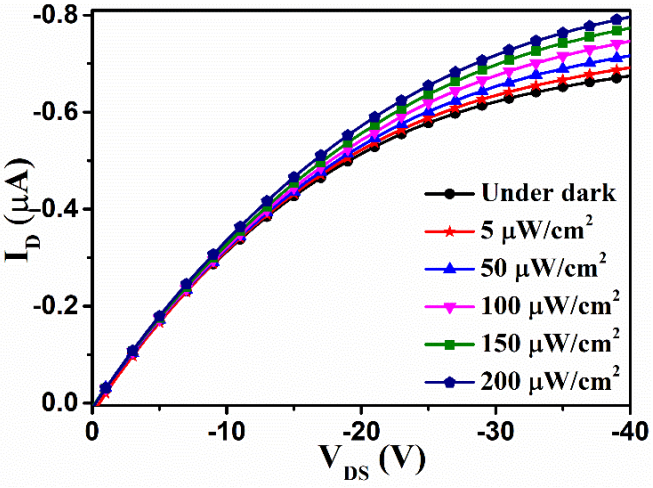

Figure 5.8: Output characteristics of the OTFT under illumination of 540 nm wavelength at different light intensity.

film has maximum optical absorbance. The output characteristics for different optical intensities but at a fixed wavelength of 540 nm are also shown in Figure 5.8. With the increase in light intensity, the generated photoexcitons are increased to result in the enhanced drain current due to enhanced charge carrier density in the OTFT channel. Thus, the drain current of the OTFT under illumination can be expressed as [83]:

$$\begin{aligned} I_{D,i} &= I_{D,d} + I_{D,p} \\ &= \frac{W}{2L}\mu C_i \left(V_{GS} - V_{th}\right)^2 + \frac{W}{L}\mu q \alpha_{eff} I_L (V_{GS} - V_{th}) \\ &= I_{D,d} + BI_L \end{aligned} \tag{5.3}$$

where $I_{D,p}$, I_L, α_{eff} and B are the photo-generated current, light intensity, photo-charge generation efficiency and ratio of photo-generated current to the light intensity, respectively.

Using the drain current Equation (5.1) in the saturation region, the OTFT parameters under the light illumination can be calculated from the transfer characteristics shown in Figure 5.9 for 200 µW/cm^2 intensity at 540 nm wavelength. Figure 5.10 shows the transfer characteristics of the OTFT under a lower intensity of 5 µW/cm^2 at 540 nm wavelength and lower drain-to-source voltage of -10 V. The photocurrent in the off-state of the transistor is observed to be increased drastically under illumination as shown in Figure 5.10. The OTFT performance parameters under dark and illumination are listed and compared in Table 5.2. The optical responsivity ($R = (I_{D,i} - I_{D,d}) / P$) shown in Figure 5.11 of the organic phototransistor under study is calculated as the change in photocurrent under optical illuminations. The maximum responsivity of 11.3 A/W is found for the light intensity of 5 µW/cm^2, which is better than that of the spin-coated PQT-12 film based phototransistor reported by others [149]. This enhanced responsivity of the FTM based phototransistor is attributed to the liquid

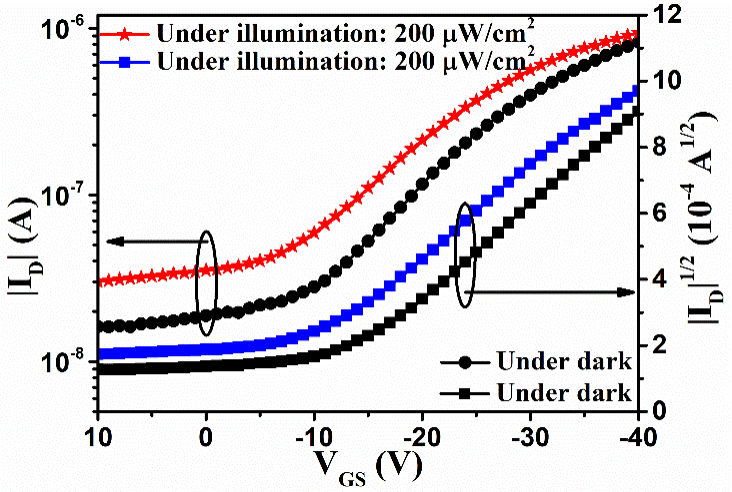

Figure 5.9: Transfer characteristics of the PQT-12 thin film based OTFT at V_{DS} = -40 V under dark and illumination of 540 nm light with an intensity of 200 µW/cm^2.

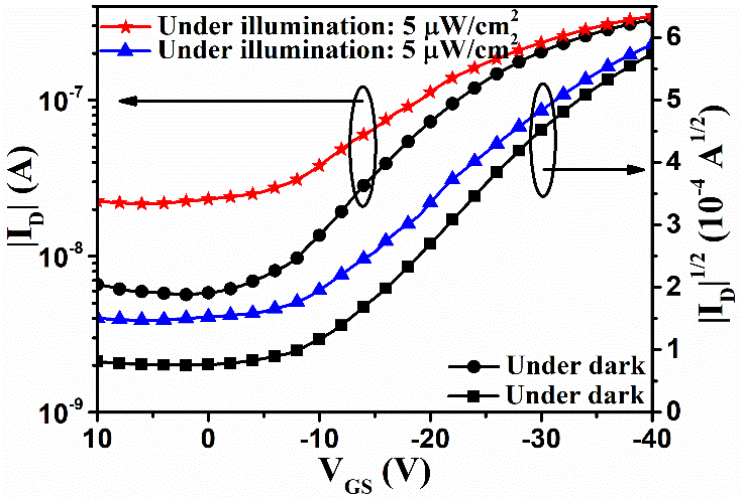

Figure 5.10: Transfer characteristics of the PQT-12 thin film based OTFT at V_{DS} = -10 V under dark and illumination of 540 nm light with an intensity of 5 μW/cm^2.

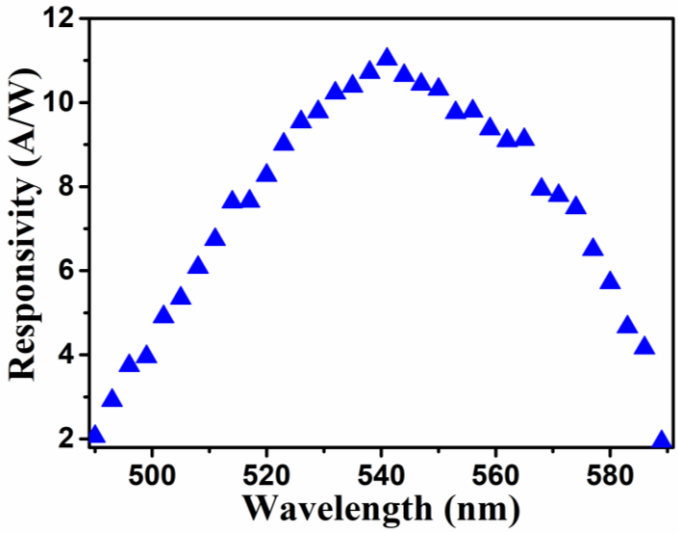

Figure 5.11: Responsivity of the PQT-12 thin film based phototransistor under illumination of 5 μW/cm^2 light intensity.

crystalline phase macromolecules structure, reduction in charge trapping density and, well aligned and self-assembled PQT-12 film [27], [28], [105], [147], [178]. The responsivity obtained is also better than other reported phototransistor based on P3OT [140] and F8B2 [139]. The optical gain of the fabricated phototransistor is calculated from the responsivity and found as 26. The performance parameters of the fabricated phototransistor are compared with the previously reported phototransistors in Table 5.3.

Table 5.2: OTFT parameters under dark and light illuminations.

OTFT parameters	**Dark condition**	**Light Illumination (200 μW/cm^2 & 540 nm)**
Field-effect mobility (cm^2/Vs)	7.8×10^{-2}	8.9×10^{-2}
Threshold voltage (V)	-8.1	-5.3

Table 5.3: Comparative list of the reported phototransistors.

References	**Responsivity (A/W)**	**Light intensity (μW/cm^2)**	**Light wavelength (nm)**	**Field effect mobility (cm^2/Vs)**	**Deposition techniques**	**Conducting polymers**
This work	11.3	5	540	7.8×10^{-2}	FTM	PQT-12
Wasapinyokul et al. [149]	6.6	3	525	1.1×10^{-3}	Spin	PQT-12
Hamilton and Kanicki [139]	0.0007-10	2900	White light	3×10^{-3}	Spin	F8T2
Wang et al. [143]	18.5	5	465	1.2×10^{-4}	Spin	F8T2
Narayan and Kumar [81]	1	1000	532	10^{-3}-10^{-4}	Spin	P3OT
Han et al. [144]	4	-	470	-	Spin	P3HT:THBT-ht
Pal et al. [53]	250	51000	White light	1×10^{-2}-7×10^{-2}	Drop cast	P3HT

5.4 Conclusion

In this chapter, the electrical and optical characteristics of the OTFT using a ~20 nm thin FTM based PQT-12 film have been investigated. Under dark condition, the FTM based OTFT under study has higher field-effect mobility and lower threshold voltage than the conventional spin-coated PQT-12 film based OTFT. The maximum absorbance of the FTM based PQT-12 film is observed at ~540 nm with side peaks at 505 and 583 nm which are attributed to the better-oriented FTM-derived PQT-12 films as compared to the conventional spin-coated PQT-12 films. Under illumination, the

drain current of the transistor increases with the light intensity due to the photo-generated excitons. The field effect mobility is increased from 7.8×10^{-2} cm^2/Vs to 8.9×10^{-2} cm^2/Vs and the threshold voltage (magnitude) is decreased from -8.1 V to -5.3 V when the illumination intensity is changed from zero (i.e. dark condition) to 200 $\mu W/cm^2$ at ~540 nm. The maximum responsivity of 11.3 A/W has been measured for 5 $\mu W/cm^2$ incident light intensity at 540 nm wavelength. Thus, the OTFT can be used for detecting the green light of the visible spectrum.